NUMERICAL STUDY ON STRUCTURAL OPTIMIZATION OF HEAT TRANSFER PERFORMANCE OF AN ECCENTRIC ELLIPTICAL CROSS-SECTION RADIAL GRAVITY HEAT PIPE

Yuhao GAO [a], Xinxin REN [a], Tianyu WU [a], Jianqiu ZHOU [a, *]

[a] School of Energy Science and Engineering, Nanjing Tech University, Nanjing, Jiangsu Province, 210000, China

[*] Corresponding author; E-mail: zhouj@njtech.edu.cn

Abstract

To address the lack of quantitative comparative studies on the coupled effects of geometric parameters on phase-change heat transfer performance in eccentric elliptical cross-sectional radial gravity heat pipes, this work systematically investigates the effects of eccentricity and elliptical cross-sectional aspect ratio on the internal temperature field distribution, flow characteristics, and total thermal resistance based on a three-dimensional two-phase flow numerical model. The results indicate that the total thermal resistance exhibits a nonlinear trend, first decreasing and then increasing with increasing eccentricity. For the investigated EE-RHP geometry with an outer tube of 60 × 40 mm and an inner tube diameter of 25 mm, an eccentricity of 10 mm yields lower wall temperatures and the lowest total thermal resistance among the investigated cases under all examined heating power conditions. Further analysis reveals that the aspect ratio influences vapor transport paths and temperature field uniformity by modifying the annular flow channel geometry; as a/b increases, the flow restriction along the minor axis becomes more pronounced, leading to a slight increase in total thermal resistance. A comprehensive comparison demonstrates that a/b = 1.25 achieves a more favorable balance between flow passage continuity and heat transfer area. These results provide quantitative guidance for the selection of structural parameters and the optimal design of eccentric elliptical cross-sectional radial gravity heat pipes.

Key words: *eccentric radial heat pipe; eccentric distance; aspect ratio of elliptical cross-section; structural optimization; numerical simulation*

1. Introduction

As a highly efficient two-phase heat transfer device, heat pipes rely on the phase change of the working fluid to achieve effective heat transport and are widely applied in waste heat recovery and high heat flux thermal management systems [1-3]. Among them, gravity-assisted heat pipes are of considerable engineering value due to their simple structure and reliable operation; however, the traditional axial configuration has gradually revealed limitations in terms of heat transfer path length and structural integration [4-6]. In this context, radial heat pipes (RHPs) shorten the heat transfer path

and reorganize the vapor–liquid flow space, thereby exhibiting clear advantages in improving temperature uniformity and system stability. Studies by Liu et al. [7], Han et al. [8], and Wang et al. [9] have demonstrated that the radial annular structure can effectively regulate vapor transport and liquid film return processes, thus reducing flow resistance and enhancing overall heat transfer performance. Furthermore, by introducing structural enhancement measures such as internal fins, coordinated optimization of two-phase flow organization and thermal resistance distribution can be further achieved [10-14]. Therefore, geometric configuration is a key factor governing the heat transfer performance of radial heat pipes.

In the structural optimization of radial heat pipes, cross-sectional geometry has gradually attracted increasing attention. Mahmood et al. [15] reported that non-circular cross-sections exhibit potential advantages in phase-change heat transfer, as heat transfer and flow characteristics can be improved by modifying the wetted perimeter distribution and flow channel geometry. Compared with circular cross-sections, elliptical cross-sections can further optimize the annular flow channel within confined spaces, enabling a synergistic enhancement of heat transfer and reduction of flow resistance. Experimental studies by Tao et al. [16] showed that elliptical gravity-assisted heat pipes outperform circular ones in terms of isothermality and overall heat transfer performance. In addition, elliptical cross-sectional structures have demonstrated favorable comprehensive thermal performance in various heat pipes and heat exchange systems [17-19], as well as certain advantages in energy utilization efficiency and thermodynamic performance [20].

Although the above studies provide valuable references for improving the performance of radial heat pipes and elliptical cross-sectional structures, most existing work has focused on symmetric configurations or single geometric parameters. Quantitative investigations on the coupled effects of multiple geometric parameters in eccentric elliptical cross-sectional radial gravity heat pipes under eccentric arrangements remain limited. In practical engineering applications, the non-uniform annular gap formed by eccentric structures can significantly reconstruct vapor transport channels and liquid film return paths, thereby affecting the overall heat transfer performance. Therefore, in this study, a three-dimensional two-phase flow numerical model of an eccentric elliptical cross-sectional radial gravity heat pipe (EE-RHP) is developed. The effects of eccentricity and elliptical cross-sectional aspect ratio on the internal flow characteristics, temperature field distribution, and total thermal resistance are systematically investigated under different heating power conditions, providing quantitative guidance for the structural parameter optimization and engineering application of EE-RHPs.

2. Model Description

2.1. Physical Model

In this study, numerical simulations of a copper-water eccentric elliptical radial heat pipe (EE-RHP) were conducted using a full-scale three-dimensional CFD model, and its physical model is shown in Fig. 1. The device consists of a 1.8 m elliptical outer tube (60×40 mm) and a 2.4 m circular inner tube (25 mm in diameter), with the eccentricity set at 10 mm. This asymmetric annular gap design is intended to optimize two-phase flow organization through spatial reconfiguration, thereby synergistically enhancing phase-change heat transfer and strengthening gravity-assisted reflux. In this work, the numerical analysis of eccentricity and aspect ratio is carried out within one fixed baseline EE-RHP configuration, so that the influence of structural variation can be evaluated under a consistent geometric

framework. The computational domain encompasses the evaporation section (heated by constant heat flux on the outer wall) and the condensation section (water-cooled inner tube). To evaluate the evolution characteristics of the wall temperature, eight monitoring points (T_1-T_8) were equidistantly arranged along the axial direction on the outer surface of the heat pipe for data collection.

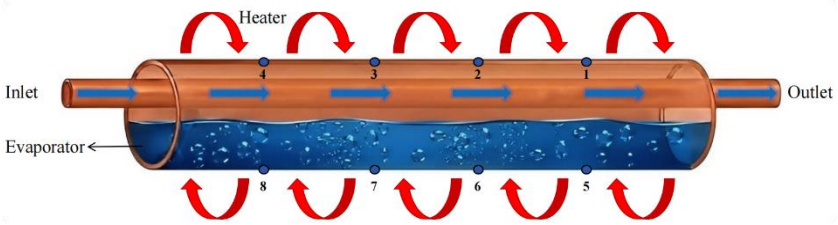

Fig. 1 Geometric Model of the EE-RHP

2.2. Governing Equations

(1) Continuity Equation

$$\frac{\partial \rho}{\partial t} + \nabla \cdot (\rho u) = 0 \tag{1}$$

Here, ρ represents density, kg/m³; u denotes the velocity vector, m/s; and t signifies time, s.

(2) Momentum Equation

$$\frac{\partial}{\partial t}(\rho u) + \nabla \cdot (\rho u u) = -\nabla p + \nabla \cdot \left[\mu\left(\nabla u + \nabla u^{\mathrm{T}} - \frac{2}{3}\mu(\nabla \cdot I)\right)\right] + \rho g + F_{\mathrm{CSF}} \tag{2}$$

Here, g is the gravitational acceleration, m/s²; P is the pressure, Pa; ρ is the density, kg/m³; μ is the dynamic viscosity, Pa·s; I is the identity tensor; F_{CSF} is the surface tension, N/m.

(3) Energy Equation

$$\frac{\partial}{\partial t}(\rho E) + \nabla \cdot (\rho E u) = \nabla \cdot (k \cdot \nabla T) + \nabla \cdot (p u) + S_E \tag{3}$$

Here, E is the energy, J; T is the temperature, K; k is the thermal conductivity, W/(m·K); S_E is the energy source term.

(4) Phase Change Equation

$$\frac{\partial(\alpha_v \rho_v)}{\partial t} + \nabla \cdot (\alpha_v \rho_v \mathrm{u}) = S_m \tag{4}$$

Here, α_v is the vapor volume fraction, and $S_m = \dot{m}_{l\to v} - \dot{m}_{v\to l}$ is the interphase mass transfer rate (defined in the UDF based on local superheat/subcooling relative to T_{sat}) ; the corresponding energy source term in Eq. (3) is coupled by latent heat as $S_E = -h_{lv} S_m$.

2.3. Initial and Boundary Conditions

To optimize computational efficiency, the initial temperature of the entire EE-RHP domain is uniformly set to 373 K. The cooling water inlet in the inner tube is set as a velocity inlet (flow velocity of 0.478 m/s, temperature of 283.15 K), and the outlet boundary condition is a pressure outlet. Heat input in the evaporation section is implemented through preset constant heat fluxes (14006.7, 17508.4, and 21010.0 W m^{-2}) on the outer wall surface to simulate thermal loads of 4, 5, and 6 kW; the condensation section utilizes convection coupling between the wall and the inner tube cooling water for heat dissipation. The saturation temperature and operating pressure are set to 373.15 K and 101325 Pa,

respectively.

2.4. Solution Methods and Strategies

In this study, all simulations are conducted using the ANSYS Fluent pressure-based solver. Transient calculations are employed to accurately simulate the phase-change process, with a fixed time step of 10^{-3} s. Mass and energy source terms during the phase change are defined through User-Defined Functions (UDFs). For the two-phase working fluid, the vapor phase is treated as an ideal gas, and the thermophysical properties of both phases are incorporated via UDFs as functions of temperature using polynomial fitting. The overall flow regime is selected as turbulent, utilizing the SST k-ω turbulence model, and the SIMPLE algorithm is adopted for pressure-velocity coupling. Additionally, the energy, momentum, and density equations are solved using first-order upwind schemes, while the PRESTO! method is used for pressure discretization. The Geo-Reconstruction scheme is employed to capture volume fractions to define the gas-liquid interface. In this research, the heat pipe is determined to have reached a steady state and the numerical calculation is considered converged when the residuals for the mass, velocity, and energy equations fall below 10^{-3}, 10^{-5}, and 10^{-9}, respectively, and the monitored parameters remain stable.

2.5. Model Validation and Grid Independence Verification

2.5.1 Model Validation

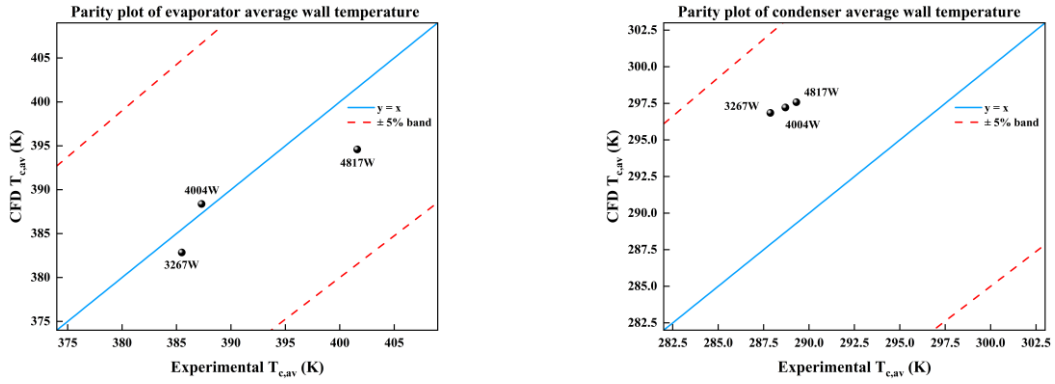

(a) (b)

Fig. 2 Model Validation

To verify the reliability of the CFD model, experimental data from the literature [5] are selected as the benchmark to validate the numerical results of the average wall temperatures in the evaporation and condensation sections. Fig. 2 above presents a parity plot of the average wall temperatures for the evaporation and condensation sections, featuring the ideal consistency reference line $y=x$ and ±5% relative deviation bands. The results indicate that under different heat input conditions, the relative deviations of the average wall temperature in the evaporation section are all less than 2% (Fig. 2a), while the relative deviations in the condensation section range between 2.7% and 3.0% (Fig. 2b). The predicted results for all conditions lie within the ±5% deviation bands. In summary, the numerical model demonstrates high accuracy and stability, providing a reliable foundation for subsequent research on the geometric parameter optimization of the EE-RHP.

2.5.2 Grid Independence Verification

To enhance the accuracy of the numerical simulation, local mesh refinement was applied at the boundaries of the evaporation and condensation sections of the EE-RHP to conduct grid independence verification. Concurrently, the wall temperatures of the evaporation section under different mesh densities were compared, as illustrated in Fig. 3. The results demonstrate that when the number of grid cells exceeds 753,000, the influence of mesh density on the simulation results becomes negligible. Consequently, a mesh count of approximately 753,000 is maintained for the models in subsequent studies.

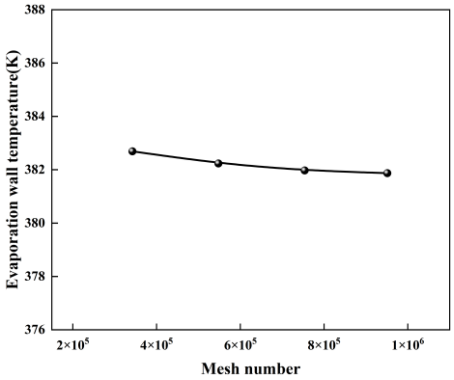

Fig. 3 Grid independence verification

3. Results and Discussion

3.1. Effect of Different Eccentricity on the Heat Transfer Performance of EE-RHP

The eccentricity alters the distribution of the annular flow channel between the inner and outer tubes, thereby directly affecting the circulation paths and heat transfer characteristics of the vapor–liquid two-phase flow inside the EE-RHP. To eliminate the influence of liquid level submerging the inner tube on the condensation process, a uniform filling ratio of 30% is adopted for all eccentric configurations in this section. Eccentricities of 2, 4, 6, 8, 10, and 12 mm are selected, and numerical simulations are performed over a heating power range of 4000-6000 W to investigate the effects of the eccentric structure on the heat transfer performance.

Fig. 4 illustrates the influence of eccentricity on the average wall temperatures of the evaporator and condenser sections of the EE-RHP.

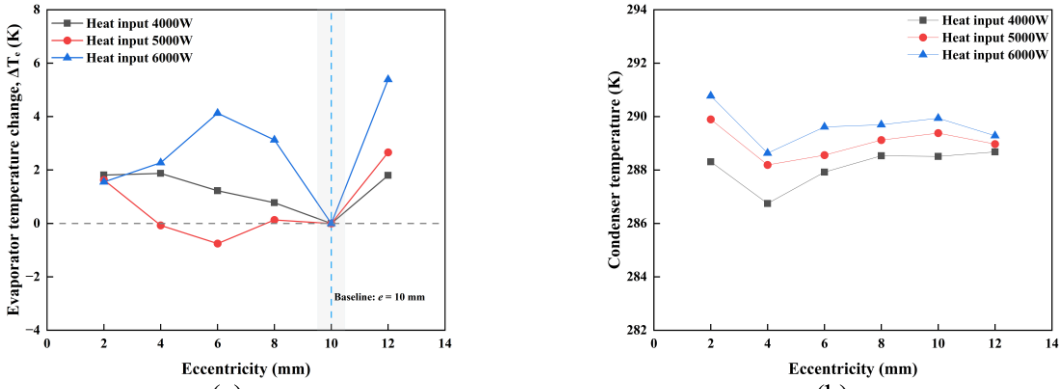

Fig. 4 Effect of eccentricity on average wall temperature: (a) Evaporator; (b) Condenser

As shown in Fig. 4(a), under heating powers of 4000 W and 6000 W, all cases except the reference

eccentricity exhibit a positive relative temperature rise, which becomes more pronounced with increasing heat input. At 6000 W, when the eccentricity reaches 12 mm, the relative temperature rise is approximately 5.39 K, indicating that an excessively large eccentricity significantly deteriorates the heat transfer performance of the evaporator under high heat-load conditions. In contrast, for eccentricities ranging from 2 to 8 mm, the variation in wall temperature is relatively small. At 5000 W, the minimum wall temperature shifts slightly from 10 mm to 6 mm; however, within the range of 4–10 mm, the wall temperature differences remain below 0.9 K, indicating that the wall temperature is insensitive to changes in eccentricity within this range and that the heat transfer performance is relatively stable. Fig. 4(b) shows that the condenser wall temperature is insensitive to variations in eccentricity, varying within the range of 286.75-290.77 K and being mainly governed by the cooling conditions.

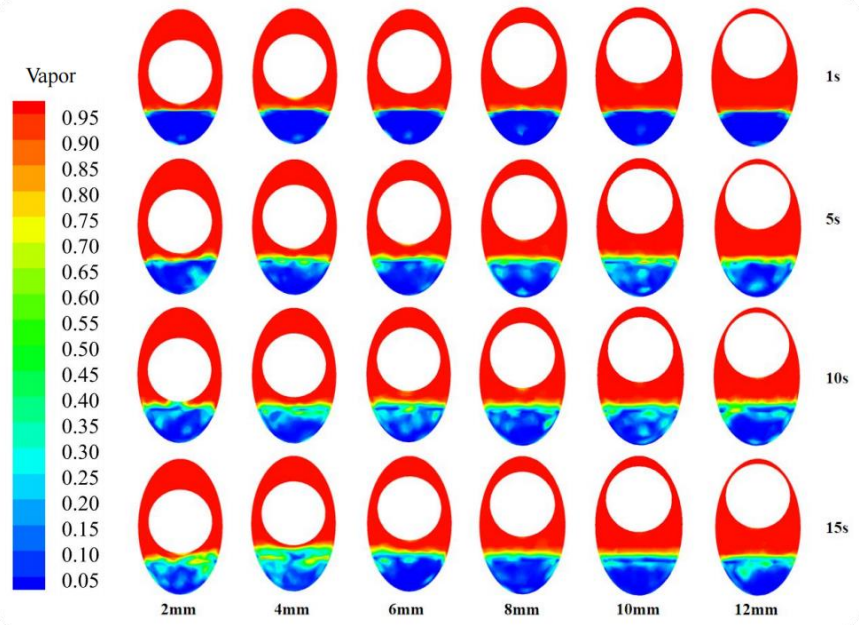

Fig. 5 Steam Volume Distribution Contour Maps at Different Time Instants for Various Eccentricity Values (30%, 5000W)

Fig. 5 presents the temporal evolution of the vapor volume fraction at different eccentricities under a heating power of 5000 W. As time progresses, the vapor region gradually expands and extends upward from the bottom. At smaller eccentricities (2-4 mm), the vapor distribution is relatively uniform and the expansion is slow, whereas at larger eccentricities (10-12 mm), the vapor region increases markedly and expands more rapidly, indicating that eccentricity has a significant influence on vapor generation and accumulation characteristics. Although the vapor volume fraction increases at larger eccentricities, its effect on the heat pipe performance is also governed by the combined influences of the evaporator wall temperature and flow characteristics.

Fig. 6 presents the steady-state temperature field distributions of the EE-RHP under different heating powers and eccentricities. In all cases, the temperature field exhibits a hot-top and cold-bottom pattern, with the highest temperature region located at the top of the outer tube due to reduced vapor velocity and heat accumulation caused by vapor convergence. As the heating power increases, both the overall temperature level and the temperature gradient increase markedly. At a fixed power, a moderate increase in eccentricity lifts the inner tube away from the bottom liquid pool and enlarges the effective condensation area, thereby improving heat transfer performance; however, when the eccentricity reaches 12 mm, the excessively narrow annular gap at the top restricts vapor transport, leading to a deterioration

of the temperature field.

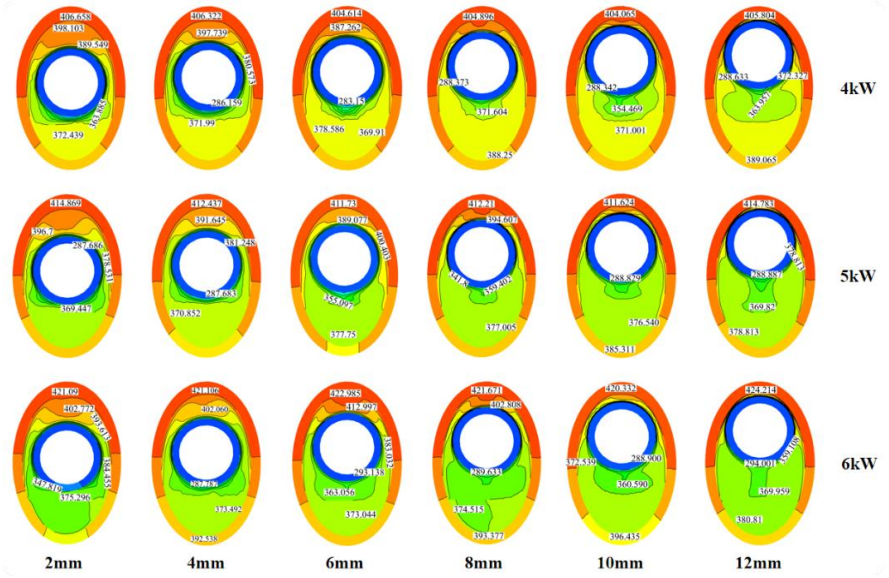

Fig. 6 Temperature contours under different heating powers and various eccentricities

Fig. 7 illustrates the axial wall temperature distribution of the evaporation section of the EE-RHP under different eccentricities.

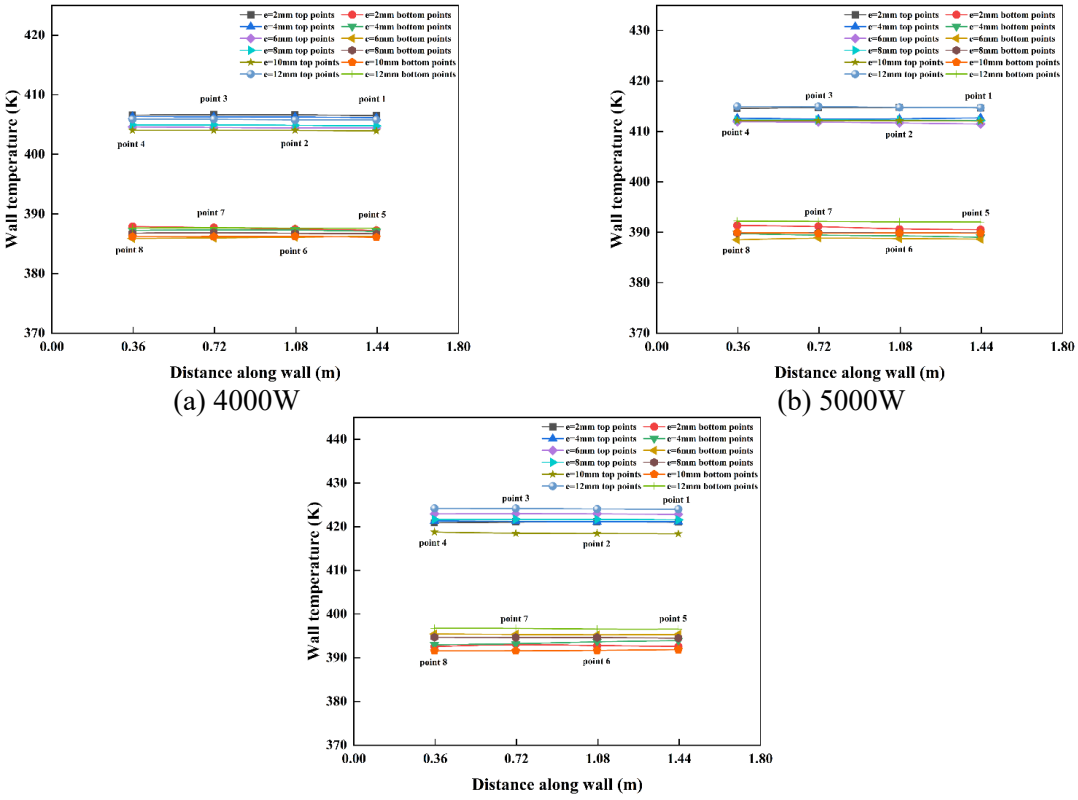

Fig. 7 Axial wall temperature distribution in the evaporation section of the heat pipe under different eccentricities

Due to flow stagnation caused by vapor convergence at the top and the relatively low thermal conductivity of the gas phase, the temperatures at the upper monitoring points (#1-#4) are higher than those at the lower monitoring points (#5-#8). As the eccentricity increases, the wall temperature distribution exhibits a U-shaped variation that first decreases and then increases. At an eccentricity of

10 mm, the temperatures of the monitoring points are overall lower; however, when the eccentricity increases to 12 mm, the top gap becomes excessively narrow, creating a flow dead zone that leads to a temperature rebound. Furthermore, the axial temperature difference between monitoring points on the same side is less than 0.8 K across all operating conditions, indicating that the eccentric structure effectively enhances radial heat transfer while maintaining excellent axial temperature uniformity.

Fig. 8 illustrates the variation in total thermal resistance of the EE-RHP under different heating powers and eccentricities. As the heating power increases, the convective heat transfer coefficients on both the evaporation and condensation sides increase simultaneously, resulting in a significant decrease in total thermal resistance and exhibiting high power sensitivity. The influence of eccentricity on the total thermal resistance is non-monotonic; at an eccentricity of 10 mm, the total thermal resistance reaches its minimum (0.02590, 0.02179, and 0.01878 K/W for 4, 5, and 6 kW, respectively), indicating that the heat pipe achieves optimal heat transfer efficiency at this parameter.

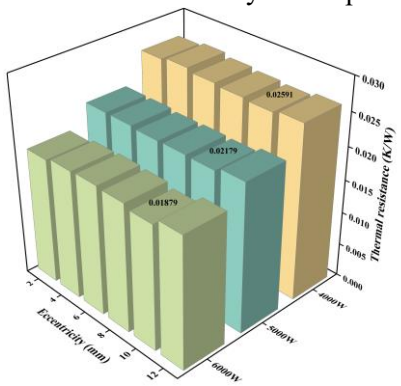

Fig. 8 Distribution of the total thermal resistance of the heat pipe at different eccentricities

In contrast, thermal resistance is higher at eccentricities of 2 mm and 12 mm, suggesting that excessively small or large eccentricities lead to flow instability or increased local thermal resistance, thereby hindering heat transfer performance. It should also be noted that the above eccentricity-dependent trends are associated with the present outer/inner cross-sectional matching, because the annular-gap distribution is jointly determined by the eccentric distance and the tube-size relation. Overall, appropriate adjustment of eccentricity effectively reduces the total thermal resistance, further verifying the critical role of the eccentric structure in improving the performance of the EE-RHP.

3.2. Effect of Elliptical Cross-Section Aspect Ratio on EE-RHP

The previous section identified an eccentricity of 10 mm as the preferred vertical spatial configuration; however, the heat transfer performance of the EE-RHP is also closely related to the elliptical cross-sectional aspect ratio a/b of the outer tube. Although increasing a/b can expand the heat transfer area along the major axis, it compresses the vapor flow channel along the minor axis and weakens the transport capability. Based on an eccentricity of 10 mm, this section investigates four aspect ratios, a/b = 1.25, 1.5, 1.75, and 2.0. Owing to geometric constraints, the circular cross-section with a/b = 1 is not considered. Given that the inner tube is fixed at an eccentricity of 10 mm and sufficient space is available at the bottom, the filling ratio is uniformly set to 50% to minimize the influence of the liquid level and to more accurately evaluate the effect of cross-sectional geometry on the heat transfer performance of the EE-RHP.

Fig. 9(a) indicates that the response of the evaporator wall temperature to the aspect ratio a/b

exhibits a pronounced heat-load dependence. At heat loads of 4-5 kW, the variation is relatively small, whereas at a high heat load of 6 kW it increases continuously with increasing a/b, reaching the maximum at a/b = 2. This behavior is mainly attributed to the fact that increasing the aspect ratio compresses the vapor flow passage along the minor axis, which significantly increases the vapor transport resistance under high heat-load conditions and consequently leads to a deterioration of the local heat transfer capability in the evaporator section.

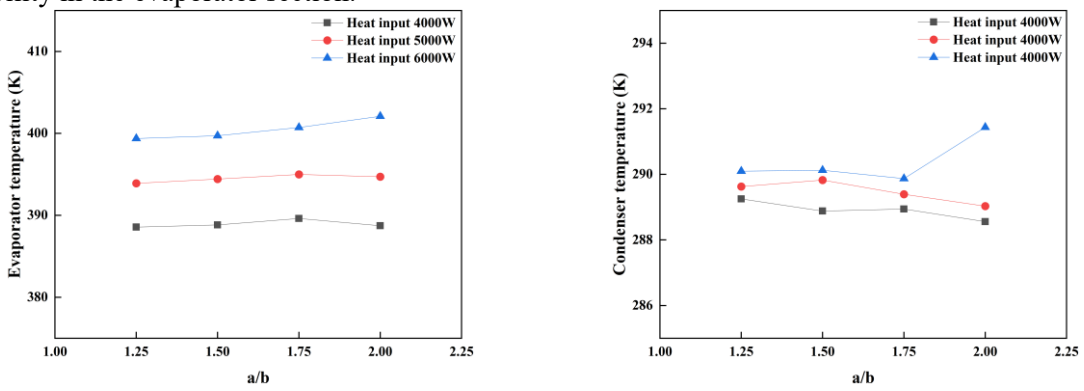

(a) (b)

Fig. 9 Variation of the average wall temperatures of the evaporator and condenser sections of the heat pipe with the cross-sectional aspect ratio

Fig. 9(b) shows that the condenser wall temperature is generally insensitive to variations in the aspect ratio, with a noticeable increase only at 6 kW and a/b = 2, indicating that under this operating condition the degradation of heat transfer in the evaporator has begun to affect the overall thermal balance of the system.

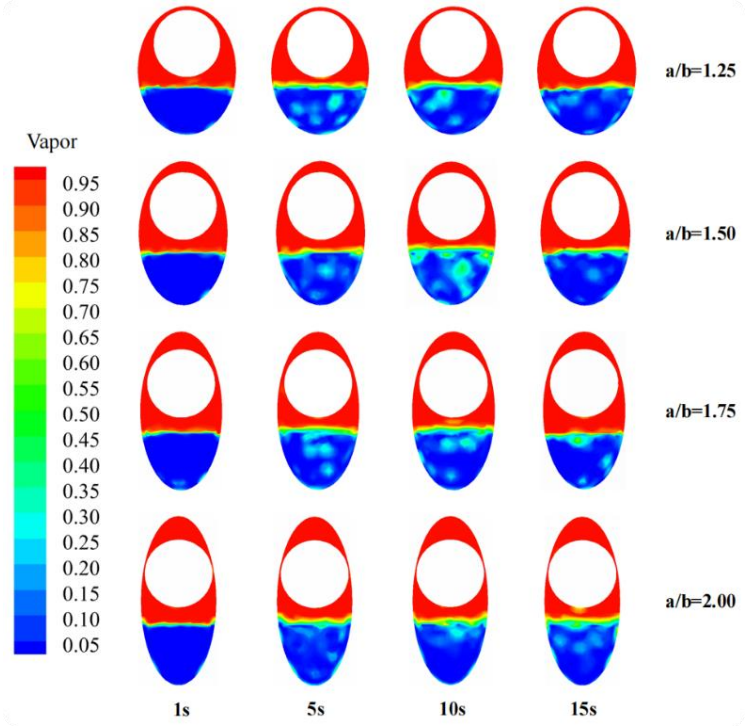

Fig. 10 Vapor volume fraction distribution contours under different aspect ratios (50%, 5000 W)

Fig. 10 illustrates the temporal evolution of the internal vapor volume fraction in the EE-RHP under different elliptical cross-section aspect ratios during the period of 1-15 s. By comparing cross-sections

with different aspect ratios at the same instant, it can be observed that when a/b = 1.25 (nearly circular), the generated bubbles can detach from the heated surface relatively freely and smoothly and rise into the vapor core. Under this condition, the internal flow resistance is minimal and the circulation process remains relatively stable.

As the aspect ratio increases, compression along the minor axis of the ellipse narrows the vertical flow passages, and the upward migration paths of the bubbles become increasingly constrained, leading to a gradual increase in flow resistance. When the elliptical cross-section becomes flattened to a/b = 2.0, the flow passages on both sides of the inner tube become excessively narrow, making it difficult for the generated vapor to migrate upward effectively. As a result, a large amount of vapor accumulates near the heated surface, forming a local vapor film. This vapor film hinders direct contact between the liquid and the heated wall, thereby causing an increase in the heat pipe wall temperature and a deterioration in heat transfer performance.

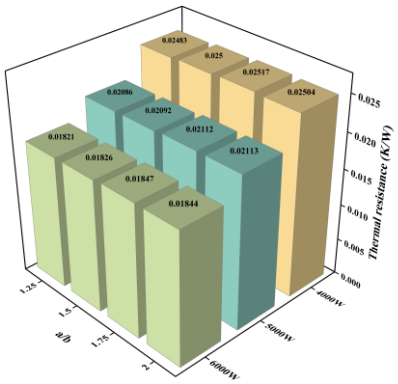

Fig. 11 Distribution of the total thermal resistance of the heat pipe at different cross-sectional aspect ratios

Fig. 11 illustrates the variation of the total thermal resistance of the EE-RHP under different heating powers and aspect ratios. For all aspect ratio cases, the total thermal resistance decreases markedly as the heat input increases from 4 kW to 6 kW, indicating that higher heat loads enhance the phase-change circulation process. In contrast, the influence of the aspect ratio on the total thermal resistance is relatively weak, with variations typically less than 0.5% under the same heat input and a slight increase observed with increasing a/b, suggesting that cross-sectional flattening introduces additional flow and heat transfer resistance to some extent. A comprehensive comparison shows that a/b = 1.25 consistently corresponds to lower total thermal resistance under all power conditions, reflecting a more favorable balance between flow passage continuity and heat transfer capability.

It should be noted that the influence of eccentricity on EE-RHP performance is closely related to the cross-sectional size matching between the outer elliptical tube and the inner circular tube. From a physical viewpoint, this geometric relation determines the distribution of the annular flow space and therefore governs both the vapor transport passage and the liquid return path. When the outer tube cross-section is relatively large compared with the inner tube, the annular gap remains sufficiently open over most of the perimeter, so the flow-field asymmetry introduced by eccentricity becomes weaker and the thermal performance becomes less sensitive to eccentricity. In contrast, when the outer and inner tube sections are too close, the local narrow-gap region caused by eccentricity may impose excessive flow resistance, hinder vapor removal from the evaporation zone, and simultaneously restrict condensate return, which is unfavorable for stable operation and may increase the overall thermal resistance. Therefore, the optimum eccentricity determined in the present study is obtained for the current geometric

configuration, and its applicability remains constrained by the cross-sectional matching between the outer and inner tubes. Similarly, the allowable outer-wall heat flux and the required cooling intensity at the inner tube side are also geometry-dependent, because both limits are closely associated with the available vapor passage, liquid reflux capacity, and phase-change balance within the annular space. The present study focuses on structural optimization for a single baseline configuration, and further investigation is still needed regarding the applicability and related operating limits of eccentric structures under different outer/inner size ratios.

3.3. Conclusions

This study systematically analyzes the heat transfer performance of eccentric elliptical cross-sectional radial gravity heat pipes (EE-RHP) under different eccentricities and aspect ratios based on three-dimensional numerical simulations. The main conclusions are as follows:

(1) For the present EE-RHP geometry and operating conditions, an eccentricity of 10 mm leads to the lowest total thermal resistance, which is 0.02590, 0.02179, and 0.01878 K/W at power levels of 4000 W, 5000 W, and 6000 W, respectively. Smaller or larger eccentricities lead to flow instability or increased local thermal resistance, resulting in reduced heat transfer performance.

(2) Increasing the aspect ratio a/b of the EE-RHP compresses the vapor flow passage, leading to a decline in the local heat transfer capability of the evaporator section. Within the present parameter range, a/b = 1.25 consistently shows lower total thermal resistance under different heat loads and provides the best overall geometric performance.

(3) Under all conditions, the total thermal resistance significantly decreases as the heating power increases, indicating that higher heat loads help improve heat transfer performance.

In conclusion, for the present geometric configuration and operating range, the combination of an eccentricity of 10 mm and an aspect ratio a/b = 1.25 provides the best overall heat transfer performance, offering a useful basis for the structural optimization of EE-RHPs.

Nomenclature

Symbols		t	time [s]
a	Semi-major axis of the elliptical cross-section [m]	T	temperature [K]
b	Semi-minor axis of the elliptical cross-section [m]	u	velocity vector [m·s^{-1}]
E	total energy [J kg^{-1}]	Greek letters	
F_{CSF}	continuum surface force [N m^{-3}]	α_v	vapor volume fraction
g	Gravity [m s^{-2}]	μ	dynamic viscosity [Pa s]
		ρ	density [kg m^{-3}]
k	thermal conductivity [W m^{-1} K^{-1}]	∇	gradient operator
P	pressure [Pa]	Subscripts	
Q	heating power [W]	av	average
q	Heat flux [W m^{-2}]	c	condenser section
R	thermal resistance [K W^{-1}]	e	evaporator section
S_E	energy source term [W m^{-3}]	sat	saturation

S_M	interphase mass transfer rate [kg·m^{-3}·s^{-1}]	w	wall

References

[1] Farahani, S. D., *et al.*, Effect of PCM and porous media/nanofluid on the thermal efficiency of microchannel heat sinks, *International Communications in Heat and Mass Transfer*, *127* (2021), pp. 105546

[2] Emam, M., *et al.*, Performance improvement of single-junction photovoltaic systems using a new design of a heat pipe-based heat sink: experimental study, *Applied Thermal Engineering*, *219* (2023), pp. 119653

[3] Sun, Y., *et al.*, Experimental study on serpentine-looped minichannel pulsating heat pipe heat exchanger with horizontal installation for full-year efficient heat recovery in air conditioning, *International Journal of Refrigeration*, (2025)

[4] Wang, Y., *et al.*, Experimental and empirical correlation study on the heat transfer characteristics of gravity heat pipes, *International Communications in Heat and Mass Transfer*, *170* (2026), pp. 110028

[5] Wang, W. W., *et al.*, Experimental and numerical investigations of a radial heat pipe for waste heat recovery, *Applied Thermal Engineering*, *154* (2019), pp. 602-613

[6] Tseng, C. Y., *et al.*, Investigation of the performance of pulsating heat pipe subject to uniform/alternating tube diameters, *Experimental thermal and fluid science*, *54* (2014), pp. 85-92

[7] Liu, M. M., Numerical simulation and analysis of heat transfer characteristics of radial heat pipes, Ph. D. thesis, Anhui University of Technology, Ma'anshan, China, 2021 (in Chinese)

[8] Han, C. L., Experimental investigation and numerical simulation on heat transfer characteristics of radial heat pipes, Ph. D. thesis, Anhui University of Technology, Ma'anshan, China, 2016 (in Chinese)

[9] Wang, W. W., *et al.*, Thermo-hydrodynamic analytical model, numerical solution and experimental validation of a radial heat pipe with internally finned condenser applied for building heat recovery units, *Energy Conversion and Management*, *219* (2020), pp. 113041

[10] Wang, W. W., Numerical study on flow and heat transfer characteristics of coaxial radial heat pipes, Ph. D. thesis, Anhui University of Technology, Ma'anshan, China, 2018 (in Chinese)

[11] Zhao, J., Design and performance investigation of hollow-sheath high-temperature heat pipes, Ph. D. thesis, University of Chinese Academy of Sciences, Beijing, 2019 (in Chinese)

[12] Zhao, J., *et al.*, Heat transfer characteristics of a concentric annular high temperature heat pipe under anti-gravity conditions, *Applied Thermal Engineering*, *148* (2019), pp. 817-824

[13] Ma, S. W., Simulation and optimization of radial heat pipe heat exchangers under different fin conditions, Ph. D. thesis, Central South University, Changsha, China, 2013 (in Chinese)

[14] Zou, L., *et al.*, Synergy investigations for the thermal transportation performance of a coaxial gravity heat pipe with internally finned in evaporator section, *International Journal of Heat and Mass Transfer, 184* (2022), pp. 122312

[15] Mahmood, S. L., Akhanda, M. A. R., Experimental investigation of micro heat pipes of different cross-sections having same hydraulic diameter, *Journal of Thermal Science, 17* (2008), 3, pp. 247-252

[16] Tao, J. R., *et al.*, Comparative experimental study on elliptical and circular gravity-assisted water heat pipes, *Modern Energy Conservation*, (1988), 1, pp. 60-62 (in Chinese)

[17] Hussein, H. M. S., *et al.*, Performance of wickless heat pipe flat plate solar collectors having different pipes cross sections geometries and filling ratios, *Energy conversion and management*, *47* (2006), 11-12, pp. 1539-1549

[18] Barrak, A. S., *et al.*, A Heat Recovery device using Oscillating Heat Pipe with circular and elliptical tubes, *International Journal of Automotive and Mechanical Engineering, 18* (2021), 1, pp. 8442-8453

[19] Rakshith, B. L., *et al.*, Thermal management performance of a novel elliptically grooved flat heat pipe system embedded with internally cooled condenser, *Energy Conversion and Management: X*, *24* (2024), pp. 100717

[20] Zhai, Y., *et al.*, Effects of Structure Parameters of Gravity-Type Heat Pipe on Heat Transfer Characteristics for Waste Heat Recovery from Mine Return Air, *Energies*, *17* (2024), 24, pp. 6495.

Paper submitted: 07 December 2025
Paper revised: 16 March 2026
Paper accepted: 08 February 2026